Functional diversity of motoneurons in the oculomotor system

Rosendo G. Hernández[a,1], Paula M. Calvo[a,1], Roland Blumer[b], Rosa R. de la Cruz[a,2], and Angel M. Pastor[a,2]

[a]Departamento de Fisiología, Facultad de Biología, Universidad de Sevilla, 41012 Sevilla, Spain; and [b]Center of Anatomy and Cell Biology, Medical Imaging Cluster, Medical University Vienna, 1090 Wien, Austria

Extraocular muscles contain two types of muscle fibers according to their innervation pattern: singly innervated muscle fibers (SIFs), similar to most skeletal muscle fibers, and multiply innervated muscle fibers (MIFs). Morphological studies have revealed that SIF and MIF motoneurons are segregated anatomically and receive different proportions of certain afferents, suggesting that while SIF motoneurons would participate in the whole repertoire of eye movements, MIF motoneurons would contribute only to slow eye movements and fixations. We have tested that proposal by performing single-unit recordings, in alert behaving cats, of electrophysiologically identified MIF and SIF motoneurons in the abducens nucleus. Our results show that both types of motoneuron discharge in relation to eye position and velocity, displaying a tonic–phasic firing pattern for different types of eye movement (saccades, vestibulo-ocular reflex, vergence) and gaze-holding. However, MIF motoneurons presented an overall reduced firing rate compared with SIF motoneurons, and had significantly lower recruitment threshold and also lower eye position and velocity sensitivities. Accordingly, MIF motoneurons could control mainly gaze in the off-direction, when less force is needed, whereas SIF motoneurons would contribute to increase muscle tension progressively toward the on-direction as more force is required. Anatomically, MIF and SIF motoneurons distributed intermingled within the abducens nucleus, with MIF motoneurons being smaller and having a lesser somatic synaptic coverage. Our data demonstrate the functional participation of both MIF and SIF motoneurons in fixations and slow and phasic eye movements, although their discharge properties indicate a functional segregation.

motoneuron | eye movements | oculomotor | abducens | vestibular

Extraocular muscles contain two types of muscle fiber according to the pattern of innervation of their parent motor axons. The most frequent corresponds to the singly innervated fiber (SIF), which is contacted by a large-diameter axon that forms the classic *en plaque* neuromuscular junction, similar to other mammalian skeletal muscles (1–3). SIFs produce, upon single-pulse excitation, a typical twitch response (1, 4, 5). The second class of extraocular muscle fiber is less numerous and corresponds to the multiply innervated fiber (MIF). These fibers are innervated by thinner axons, which establish multiple synaptic boutons *en grappe* extending along the whole length of the fiber (1–3, 6). In contrast to SIFs, single-pulse excitation of MIFs is not followed by a strong twitch but by a slow tension that builds up upon repetitive stimulation (1, 7–9). The presence of MIFs in mammals is extremely rare (10). Electrophysiological, histochemical, and ultrastructural features of these two types of muscle fibers correlate well with their different contractile properties (11–13).

Extraocular muscle SIFs and MIFs are innervated by motoneurons located in three brainstem nuclei: the abducens, the trochlear, and the oculomotor nuclei. The proportion of MIF motoneurons is close to 20% with respect to the total population of motoneurons in each extraocular motoneuronal pool, as has been reported in monkeys (14) and rats (15). Retrograde tracer injections in primates into the distal portion of the muscle, aimed to label only MIF axons, have shown an anatomic segregation between MIF and SIF motoneurons, with MIF motoneurons located peripherally,

whereas SIF motoneurons are distributed within the boundaries of the extraoculomotor nuclei (16, 17). Similar findings have been obtained in humans (18). In the rat, there is also some segregation, although less conspicuous (15). In the cat, the anatomical location of MIF vs. SIF motoneurons has been studied only for medial rectus motoneurons, which also show certain differences in their distribution pattern (19).

Experiments using retrograde transneuronal rabies virus or anterograde tracers have revealed some differences in the origin of afferents impinging upon MIF or SIF extraocular motoneurons. In particular, the anterograde labeling in monkeys of the lateral vestibular complex labels projections only to SIF motoneurons of the oculomotor nucleus, whereas pretectal injections label terminals only over MIF motoneurons of the oculomotor nucleus. Anterograde injections into either the abducens nucleus or the parvocellular medial vestibular nucleus, or Y group, label terminals in both MIF and SIF motoneurons of the oculomotor nucleus (20). More recently, the retrograde transneuronal transfer of rabies virus injected into the distal portion of the lateral rectus muscle of primates (containing the *en grappe* terminals of MIF motoneurons) have revealed some monosynaptic inputs to MIF abducens motoneurons: the supraoculomotor area, the central mesencephalic reticular formation, and portions of the medial vestibular and prepositus nuclei (21). In summary, MIF motoneurons have been shown to receive preferentially inputs from nuclei encoding eye position or slow eye movements, whereas SIF motoneurons are innervated by all known synaptic inputs to these motoneurons (20–23). These findings suggest that MIF and SIF motoneurons could be functionally segregated depending on the type of eye movement. Thus, it has been suggested that MIF motoneurons would contribute

Significance

Extraocular muscles have multiply innervated muscle fibers (MIFs, slow or nontwitch fibers) in addition to the classic singly innervated muscle fibers (SIF). Based on anatomical studies, it has been suggested that MIF motoneurons would assist in gaze holding and slow eye movements, whereas SIF motoneurons would participate in the whole repertoire of eye movements. We have tested that proposal in alert, behaving cats with electrophysiological identification of MIF and SIF motoneurons. Our results indicate that both motoneuronal types present a tonic–phasic discharge, and fire during all types of eye movements. However, MIF motoneurons show lower thresholds, lower eye-related sensitivities, and a reduced firing level as compared with SIF motoneurons, suggesting a role in the fine alignment of gaze.

[1]R.G.H. and P.M.C. contributed equally to this work.

[2]To whom correspondence may be addressed. Email: rmrcruz@us.es or ampastor@us.es.

NEUROSCIENCE

mainly to slow eye movements and fixations, but not to saccades (fast eye movements), whereas SIF motoneurons would participate in all types of eye movements (20–23). However, oculomotor neuron activity recorded in alert animals (monkeys and cats) have shown that all motoneurons participate in all classes of eye movement (24–27). Therefore, whether the two motoneuronal populations have distinct functions is still at debate.

The aim of the present work has been to characterize the discharge activity of electrophysiologically identified MIF and SIF motoneurons of the abducens nucleus in awake, behaving cats. We have also evaluated the distribution pattern, cell size, and synaptic coverage of MIF versus SIF motoneurons. Our data demonstrate that both MIF and SIF motoneurons display a tonic–phasic discharge pattern during different types of eye movement, slow and fast, and during fixations. However, MIF motoneurons showed lower firing rates, lower thresholds, and lower eye position and velocity sensitivities than SIF motoneurons. These data suggest that MIF motoneurons should contribute to smoothly increment muscle force leading to small, but essential, adjustments of eye position required for the precise control of gaze in the entire repertoire of eye movements.

Results

Electrophysiological Identification of SIF and MIF Motoneurons.
To discern MIF and SIF motoneurons, we implanted two stimulating electrodes: one at the VIth nerve (Fig. 1A, St. 1) and the other at the myotendinous junction of the lateral rectus muscle (Fig. 1A, St. 2). Both motoneuronal types were antidromically activated following the electrical stimulation to the VIth nerve (Fig. 1 B and C, Left). However, only MIF motoneurons were antidromically activated from the electrode placed at the muscle insertion (Fig. 1 B and C, Right). Whenever a unit was isolated, we applied systematically the collision test between the orthodromic (spontaneous) spike and the antidromic spike, to assure that the isolated unit was indeed the recorded one (Fig. 1 B and C).

We measured the antidromic activation latency of SIF and MIF motoneurons as the time interval between the onset of the stimulus artifact after VIth nerve stimulation (arrows in Fig. 1 B and C) and the negative peak of the spike. The distribution of antidromic latencies shows that, although the ranges overlapped (0.499–0.825 ms for SIF motoneurons, and 0.596–0.834 ms for MIF motoneurons), most MIF motoneurons showed longer antidromic latencies than SIF motoneurons (Fig. 1D). Indeed, we found that SIF motoneurons ($n = 104$) had a lower antidromic latency (0.666 ± 0.006 ms) than MIF motoneurons (Fig. 1E) [$n = 51$, 0.717 ± 0.007 ms; $t(153) = -5.090$, $P < 0.001$, t test].

Discharge Characteristics of SIF and MIF Motoneurons During Spontaneous Eye Movements.
SIF and MIF motoneurons discharged according to a tonic–phasic firing pattern during spontaneous eye movements, as previously reported for abducens neurons (24, 26, 27). Thus, both motoneuronal types presented a stable firing during eye fixations that increased monotonically as the eye deviated more in the on-direction (temporal), which was that ipsilateral to the recording site (in our case, toward the left). Moreover, during rapid eye movements (saccades), SIF and MIF motoneurons discharged a burst of action potentials for on-directed saccades, whereas they silenced or showed an abrupt drop in firing for off-directed saccades. This tonic–phasic behavior can be readily appreciated in Fig. 2A for a SIF motoneuron, and in Fig. 2B for a MIF motoneuron. However, it should be emphasized that, even from a qualitative inspection of SIF and MIF motoneuronal discharge, there were differences between both cell types. The more conspicuous differences were the lower firing rate of MIF motoneurons in comparison with SIF motoneurons, and the presence of low-frequency bursts during on-directed saccades for MIF motoneurons, whereas SIF motoneurons displayed bursts of high frequency for on-directed saccades. In contrast, both motoneuronal types
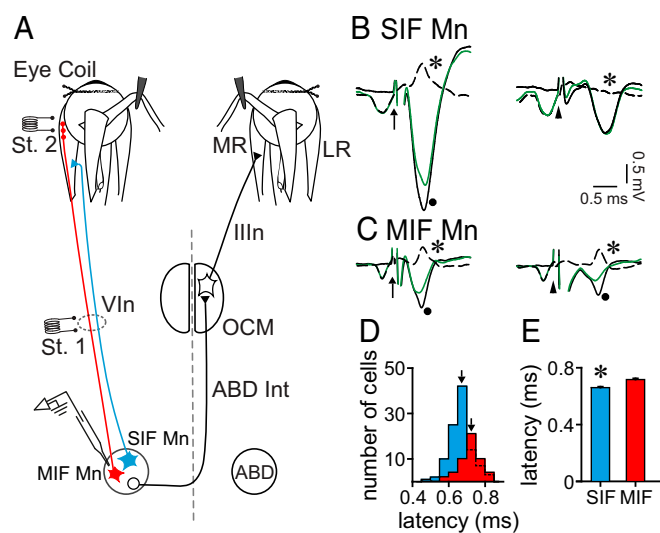

Fig. 1. Electrophysiological identification of SIF and MIF motoneurons. (A) Diagram of the experimental design. SIF and MIF motoneurons (Mn) of the abducens nucleus (ABD) were antidromically activated from the electrode (St. 1) located at the VIth nerve (VIn). Only MIF motoneurons were activated from the electrode placed at the myotendinous junction (St. 2) of the lateral rectus (LR) muscle. Abducens internuclear neurons (Abd Int) projecting to the oculomotor nucleus (OCM) are also shown. (B) Collision test of a SIF Mn. Arrow points to the stimulus artifact from the VIth nerve (St. 1 in A) and arrowhead points to the stimulus artifact from the miotendinous junction (St. 2 in A). (Left) The spike is collided after VIth nerve stimulation when the orthodromic spike discharges at a short time interval before the stimulus. The dot indicates the full antidromic field potential of ABD (black solid trace); the green trace shows the antidromic failure after conditioning with an orthodromic spike. The dashed trace is the substraction of the aforementioned traces showing an inverted spike as a result (asterisk). (Right) Lack of collision after stimulus application to the LR tendon (arrowhead) revealing no difference after subtraction of the antidromic fields (asterisk). (C) Same as B but for a MIF motoneuron. In this case, the spike was collided from both the VIth nerve (Left) and the LR insertion (Right). (D) Graph showing the distribution of antidromic latencies from the VIth nerve of MIF (red) and SIF Mn (blue) clustered at time intervals of 0.05 ms. Arrows point to the mean antidromic latency for each population. (E) Bar chart illustrating the mean and SEM of the antidromic latencies from the VIth nerve of SIF (blue) and MIF (red) Mn. Asterisk indicates significant difference between both groups ($n = 104$ and 51 SIF and MIF Mn, respectively; $P < 0.001$, t test).

exhibited a clear pause or decrease in firing rate for off-directed saccades (Fig. 2 A and B).

To evaluate the static and dynamic components of firing rate, we correlated firing rate during eye fixations versus eye position, and firing rate during saccades (previous substraction of the eye position component) (Materials and Methods) versus eye velocity. The plot corresponding to the rate-position regression line of the SIF motoneuron shown in Fig. 2A is represented in Fig. 2C (blue line and dots). The slope of the regression line corresponds to the eye position sensitivity for that cell (k_s), which was 6.4 spikes per second per degree. In contrast, the regression line of the rate-position plot for the MIF motoneuron shown in Fig. 2B yielded a much lower eye position sensitivity ($k_s = 2.1$ spikes per second per degree) (Fig. 2C, red dots and line). The graph (Fig. 2C) also illustrates, for each motoneuron, the parameter F_0 (i.e., the firing rate at straight-ahead gaze), which was also higher for the SIF motoneuron. The recruitment threshold was also calculated from the rate-position plots as the intercept of the regression line with the abscissa axis. As observed in Fig. 2C, the threshold for the MIF motoneuron (in red) was lower (i.e., fired earlier) than that of the SIF motoneuron (in blue).

Similarly, when we represented firing rate (FR) [minus the eye position (EP) component, FR − k_s·EP] versus eye velocity (EV) during saccades, we obtained a linear regression line whose slope
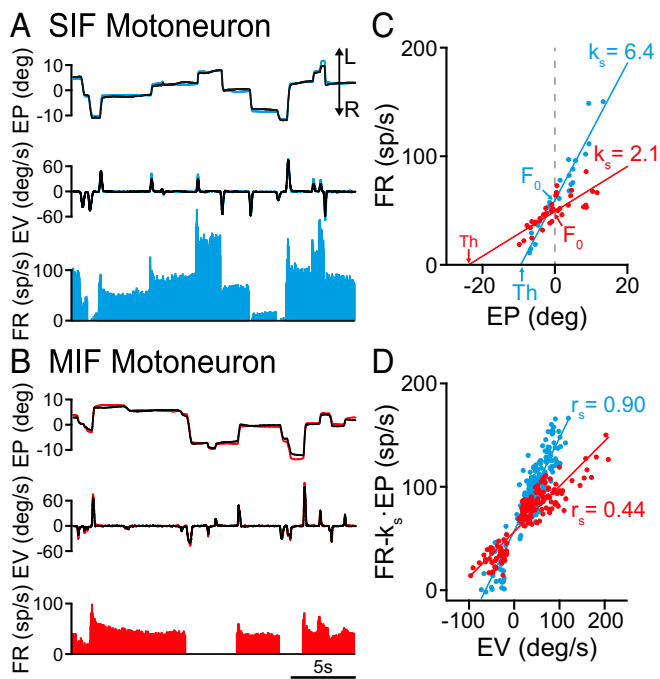
Fig. 2. Discharge of SIF and MIF motoneurons during spontaneous eye movements. (*A*) Firing rate of a SIF motoneuron during spontaneous eye movements. From top to bottom are illustrated: eye position (EP; left eye is shown in blue and right eye in black), eye velocity (EV), and firing rate of the cell (FR). L and R indicated leftward and rightward eye movement, respectively. (*B*) Same as *A* but for a MIF motoneuron (left eye position in red). (*C*) Linear regression lines obtained during fixations between firing rate and eye position (left, ipsilateral eye) for the SIF motoneuron shown in *A* (blue line and dots; correlation coefficient $r = 0.96$), and for the MIF motoneuron shown in *B* (red line and dots; $r = 0.79$). The plots also illustrate the firing rate at straight-ahead gaze (F_0, the ordinate intercept, by gray dashed vertical line), the position threshold (Th, the abscissas intercept) and their respective k_s values (the slopes). (*D*) Linear regression lines obtained during saccades between firing rate (minus the eye position component, FR $- k_s \cdot$EP) and eye velocity for the SIF motoneuron shown in *A* (blue line and dots; $r = 0.91$), and for the MIF motoneuron shown in *B* (red line and dots; $r = 0.91$). The value of r_s (slope of the firing-velocity plot) is indicated for each motoneuron.

corresponds to the neuronal eye velocity sensitivity (r_s). These rate–velocity regression lines are illustrated in Fig. 2*D*, demonstrating that the SIF motoneuron of Fig. 2*A* exhibited an eye velocity sensitivity (blue dots and line in Fig. 2*D*) ($r_s = 0.90$ spikes per second per degree per second) higher than the MIF motoneuron of Fig. 2*B* (red dots and line in Fig. 2*D*) ($r_s = 0.44$ spikes per second per degree per second).

For an assessment of pool properties, the correlations between firing rate and eye position or velocity were plotted for the entire population of SIF ($n = 104$) and MIF motoneurons ($n = 51$) analyzed (Fig. 3*A*). The plot shows that MIF motoneurons (Fig. 3*A*, in red) had, in general, lower slopes (i.e., lower eye position sensitivities, k_s) than SIF motoneurons (Fig. 3*A*, in blue). Moreover, MIF motoneurons displayed lower thresholds than SIF motoneurons (Fig. 3*A*). A conspicuous difference between both motoneuronal types can be also appreciated regarding the rate–velocity plots (Fig. 3*B*). Thus, our sample of MIF motoneurons (Fig. 3*B*, in red) demonstrated lower slopes (i.e., lower eye velocity sensitivities, r_s) than the SIF motoneurons (Fig. 3*B*, in blue).

In a next step we compared statistically these eye-related parameters to test whether there were significant differences between SIF and MIF motoneurons. Results are shown in Fig. 3 *C–F*. Regarding eye position sensitivity (k_s) (Fig. 3*C*), SIF motoneurons showed a mean k_s of 6.17 ± 0.19 spikes per second per degree,

whereas that of MIF motoneurons ($k_s = 3.13 \pm 0.15$ spikes per second per degree) was significantly lower (Fig. 3*C*) [$t(153) = 10.604$, $P < 0.001$, t test]. The same happened for firing rate at zero eye position (F_0), which was also significantly lower for the MIF motoneuronal population compared with SIF motoneurons (Fig. 3*D*) [$t(153) = 2.524$, $P = 0.013$, t test]. The eye position at which the unit was recruited into activity (threshold) was $-7.19 \pm 0.31°$ and $-11.94 \pm 0.64°$ for SIF and MIF motoneurons, respectively, the difference being significant (Fig. 3*E*) [$t(153) = 7.537$, $P < 0.001$, t test]. Thus, MIF motoneurons were recruited at eye positions more in the off-direction than SIF motoneurons. Finally, the eye velocity sensitivity (r_s) was also significantly lower for MIF motoneurons, compared with SIF motoneurons (0.47 ± 0.02 vs. 0.68 ± 0.02 spikes per second per degree per second, respectively) (Fig. 3*F*) [$t(153) = 6.761$, $P < 0.001$, t test].

We found no significant differences in the correlation coefficients obtained from the rate-position and rate-velocity plots between SIF and MIF motoneurons [for k_s: $r = 0.84 \pm 0.009$ and $r = 0.85 \pm 0.013$, respectively; $t(153) = -0.374$, $P = 0.709$; for r_s: $r = 0.79 \pm 0.010$ and $r = 0.80 \pm 0.014$, respectively; $t(153) = -0.717$, $P = 0.475$]. These data reinforce the presence of an eye position and an eye velocity sensitivity in both motoneuronal types.

We compared the performance of MIF and SIF motoneurons during saccades. Latency of peak firing after the onset of the saccade occurred in average 15 ms earlier in SIF (51.8 ± 1.0 ms) compared with MIF (67.11 ± 1.8 ms) motoneurons [$t(163) = 7.456$, $P < 0.001$]. Thus, SIF motoneurons fired maximally 16.9 ms before the peak of saccadic velocity [paired t test; $t(82) = 17.704$; $P < 0.001$]. In contrast, MIF motoneurons fired maximally only 3.8 ms in advance to peak saccadic velocity [paired t test; $t(81) = 2.554$; $P = 0.013$]. Therefore, MIF motoneurons likely are more influential during the termination phase of the saccade, whereas SIF motoneurons are
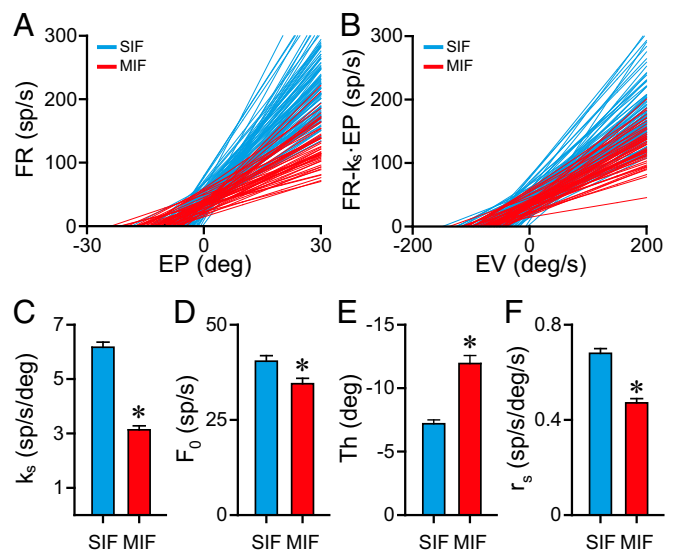
Fig. 3. Comparison of eye-related parameters during spontaneous eye movements between SIF and MIF motoneurons. (*A*) Linear regression lines of firing rate versus eye position for 104 SIF (blue) and 51 MIF (red) motoneurons. The slope of each line represents the neuronal eye position sensitivity (k_s) during spontaneous eye movements. (*B*) Linear regression lines of firing rate versus eye velocity for the same set of cells as shown in *A*. The slope of each line represents the neuronal eye velocity sensitivity (r_s) during spontaneous eye movements. (*C–F*) Bar charts comparing eye position sensitivity (k_s, in *C*), firing rate at straight-ahead gaze (F_0, in *D*), eye position threshold (Th, in *E*) and eye velocity sensitivity (r_s, in *F*) between the 51 MIF and 104 SIF motoneurons illustrated in *A* and *B*. Data are mean and SEM. Asterisks indicate significant differences ($P < 0.05$, t test).

relevant for the initial pulse that overcomes the viscoelastic forces of the orbit.

Correlations Between Motoneuronal Parameters. The positive correlation between sensitivities and threshold is another pool property of abducens motoneurons (24, 26–28). We found that k_s correlated positively with threshold for both SIF and MIF motoneurons. Thus, abducens SIF motoneurons demonstrated a significant ($r = 0.671$, $P < 0.001$) exponential correlation between k_s and recruitment threshold (Fig. 4A, blue dots and curve). The same also happened for the MIF population (Fig. 4A, red dots and curve) ($r = 0.660$, $P < 0.001$). As expected, when treating SIF and MIF motoneurons as a single population, k_s correlated exponentially with threshold (Fig. 4A, black curve) ($r = 0.754$, $P < 0.001$). In contrast, when r_s was plotted versus threshold, neither SIF nor MIF motoneurons demonstrated significant correlations, but together, the entire motoneuronal population did show a correlation between r_s and threshold (Fig. 4B) ($r = 0.402$; $P < 0.001$). k_s also correlated positively with r_s, so that motoneurons with higher k_s tended to have also higher r_s (Fig. 4C). This relationship was present for SIF (Fig. 4C, blue dots and curve) ($r = 0.498$, $P < 0.001$), for MIF (Fig. 4C, red dots and curve) ($r = 0.619$, $P < 0.001$) and for the entire pool (Fig. 4C, black curve) ($r = 0.628$, $P < 0.001$). Thus, when k_s, threshold, and r_s were plotted altogether (Fig. 4D), MIF and SIF motoneurons appeared as two distinguishable pools with some overlap: MIF motoneurons were characterized by lower k_s, lower threshold and lower r_s values compared with SIF motoneurons (compare MIF, red dots, with SIF, blue dots, motoneurons in Fig. 4D).

We found an inverse relation between k_s and antidromic latency (i.e., higher k_s correlates with lower latencies) that was significant ($P = 0.002$), although with a low correlation coefficient ($r = 0.25$), as previously reported (26). The same happened for the relationship between threshold and antidromic latency (higher threshold, lower latency; $P = 0.035$, $r = 0.169$). These two relationships (k_s and threshold vs. latency) were obtained in the whole motoneuronal pool (MIF + SIF motoneurons). Because conduction velocity (inversely related with antidromic latency) reflects cell size, it might indicate that motoneurons with the lowest conduction velocity (longer latencies) would be those of smaller size, in turn, having lower k_s and threshold values as they would recruit first according to the size principle (29). According to our data, those should be the MIF motoneurons.

In contrast, when we analyzed these same relationships only in the MIF or in the SIF motoneuron pools, no significant correlation was found. The reason may lay on the fact that MIF and SIF motoneurons appeared segregated based on these parameters; that is, MIF motoneurons were those with lower k_s and threshold, whereas SIF motoneurons were those with higher k_s and higher threshold, so that only when the two types of motoneurons were grouped as a single pool the above-mentioned relationships appeared.

Behavior of MIF and SIF Motoneurons During Spontaneous Disjunctive Eye Movements. On occasions, cats perform spontaneously disjunctive eye movements in the horizontal plane. We investigated how SIF and MIF abducens motoneurons behaved during these spontaneously occurring vergence eye movements ($n = 75$ and 41 SIF and MIF motoneurons, respectively). A variety of responses were found during disjunctive eye movements for both cell types. Thus, many SIF and MIF motoneurons fired appropriately during vergence; that is, their firing rate increased during divergences and decreased during convergences, as expected for abducens motoneurons (Fig. 5A), although with different percentages depending on the cell type ($30.6 \pm 6.9\%$ and $49.9 \pm 7.1\%$ for SIF and MIF motoneurons) (Fig. 5D). Intriguingly, some motoneurons showed a variable behavior during different episodes of nonconjugate eye movements. For example, during divergent eye movements, their firing frequency sometimes increased, whereas on other occasions, they decreased or did not even change. This happened for both SIF ($61.9 \pm 4.8\%$) (Fig. 5D) and MIF motoneurons ($40 \pm 4.2\%$) (Fig. 5D), as observed in Fig. 5B for an example of a SIF motoneuron. Other less frequent behaviors included cells that did not respond to vergence eye movements (SIF = $5 \pm 1.8\%$; MIF = $7.5 \pm 7.5\%$) (Fig. 5D), as well as those that showed an inappropriate (i.e., opposite than expected) behavior (SIF = $2.4 \pm 1.4\%$; MIF = $2.5 \pm 2.5\%$) as shown in Fig. 5 C and D. In summary, both SIF and MIF abducens motoneurons responded to vergence eye movements according to four possible types of profiles: appropriate, variable, nonresponding, and inappropriate. This variety of responses is not surprising according to previous data showing that abducens motoneurons can discharge with independent movements of either eye (binocular units), whereas others discharge monocularly with one or the other eye (monocular units) (30).

As observed in the bar chart of Fig. 5D, we evaluated the possibility of statistical differences between groups (two-way ANOVA test; the two factors were cell type—SIF or MIF—and cell response to vergence). We found that the percentage of abducens motoneurons responding appropriately during vergence eye movements was significantly higher for MIF than for SIF motoneurons, whereas the percentage of SIF motoneurons showing a variable behavior was significantly higher than that of MIF motoneurons [$F_{(1, 3)} = 5.501$; $P = 0.005$] (Fig. 5D). On the other hand, the percentage of motoneurons that did not modulate or even modulated inappropriately during vergence was similar between SIF and MIF motoneurons (Fig. 5D). Despite these differences in percentages, it is important to highlight that both SIF and MIF motoneurons showed the same patterns of behavior
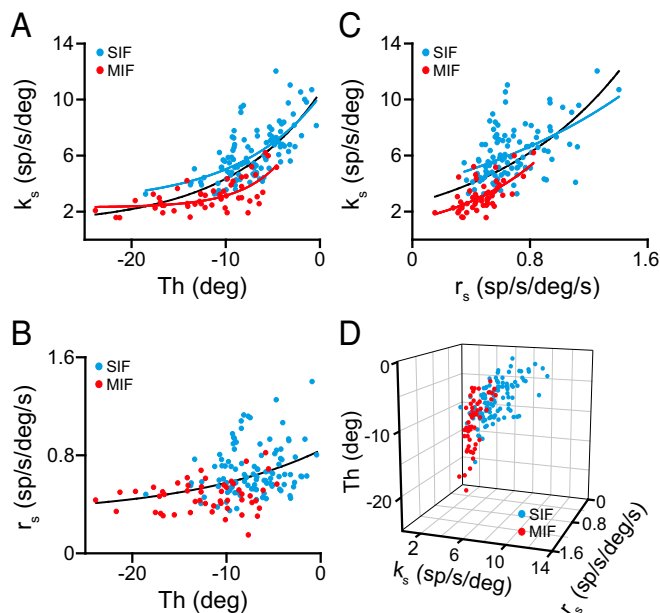

Fig. 4. Relationships of SIF and MIF eye-related sensitivities with recruitment threshold during spontaneous eye movements. (A) Plots of eye position sensitivity (k_s) versus threshold (Th) for 104 SIF (blue) and 51 MIF (red) motoneurons and for the whole population (SIF + MIF) of motoneurons (black line). Lines are the exponential regressions $y = 2.587 + 7.642 \cdot e^{0.114x}$ ($r = 0.671$, $P < 0.001$), $y = 2.302 + 8.838 \cdot e^{0.235x}$ ($r = 0.660$, $P < 0.001$), and $y = 0.998 + 9.491 \cdot e^{0.104x}$ ($r = 0.754$, $P < 0.001$) for SIF, MIF, and all motoneurons, respectively. (B) Same as A, but for eye velocity sensitivity (r_s). A significant regression was obtained only when all of the motoneurons were grouped together (black line; $y = 0.306 + 0.534 \cdot e^{0.069x}$; $r = 0.402$, $P < 0.001$). (C) Exponential regressions between eye position (k_s) and eye velocity (r_s) sensitivities for 104 SIF (blue; $y = 3.774 \cdot e^{0.708}$; $r = 0.498$, $P < 0.001$), 51 MIF (red; $y = 1.411 \cdot e^{1.642x}$; $r = 0.619$, $P < 0.001$) and for the entire population of motoneurons (black line; $y = 2.587 \cdot e^{1.094x}$; $r = 0.628$, $P < 0.001$). (D) Scatterplot of k_s, r_s, and threshold for SIF ($n = 104$, blue dots) and MIF ($n = 51$, red dots) motoneurons.
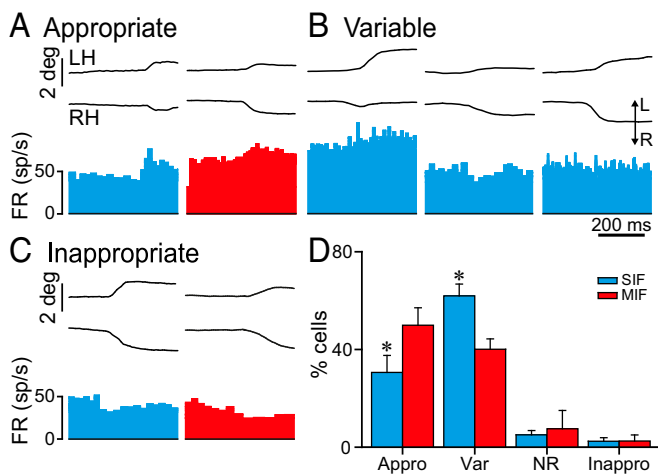
Fig. 5. Behavior of SIF and MIF motoneurons during spontaneous disjunctive eye movements. (*A*) Examples of a SIF (blue) and a MIF (red) motoneuron showing an appropriate increase in firing rate during a divergent eye movement. Recordings (*A–C*) were made on the left abducens nucleus. In *A–C*, from top to bottom: eye position of the left (LH) and right eye (RH) and firing rate (FR). (*B*) A SIF motoneuron showing different firing patterns during divergent eye movements. (*C*) Inappropriate decrease in firing of a SIF (blue) and a MIF (red) motoneuron during divergent eye movements. (*D*) Bar chart representing the percentages of SIF (*n* = 75) and MIF (*n* = 41) motoneurons behaving during nonconjugated eye movements according to one of these four types: appropriately (Appro), with a variable pattern (Var), showing no response (NR), or inappropriate (Inappro). Asterisks indicate significant differences: *P* = 0.013 for the appropriately responding group, and *P* = 0.06 for the variable-responding group (two-way ANOVA).

during vergence eye movements and, therefore, there was no a separation of functions between both motoneuronal types.

Discharge Characteristics of SIF and MIF Motoneurons During Vestibularly Induced Eye Movements. The behavior of MIF and SIF motoneurons was also studied during sinusoidal rotation of the table around the vertical axis. An example of a SIF motoneuron discharging during vestibularly induced eye movements is illustrated in Fig. 6*A*, showing that its firing rate modulated during both the slow and fast phases of the vestibular nystagmus, with the on-direction corresponding to eye displacements toward the ipsilateral side (left in our case). MIF motoneurons modulated similarly during vestibular stimulation (Fig. 6*B*). The sensitivities to eye position (k_v) and eye velocity (r_v) during vestibular stimulation were calculated by multiple regression analysis. The partial regression plots were elaborated after the substraction of the complementary component. Thus, an eye position sensitivity (k_v) was revealed after subtracting the velocity (EV) component ($r_v \cdot EV$) (Fig. 6*C*) to firing rate. In a similar way, an eye velocity sensitivity (r_v) appeared in the partial plot (Fig. 6*D*) of firing rate—minus the eye position component ($k_v \cdot EP$)—versus eye velocity. Therefore, both SIF and MIF motoneurons exhibited an eye position and an eye velocity sensitivity during vestibular eye movements. When comparing eye position sensitivity (k_v) between SIF and MIF motoneurons, a significant difference appeared with MIF motoneurons showing lower k_v values (6.18 ± 0.29 vs. 3.44 ± 0.23 spikes per second per degree, *n* = 81 and *n* = 40, for SIF and MIF motoneurons, respectively) (Fig. 6*E*) [*t*(119) = 6.117, *P* < 0.001, *t* test]. Similarly, r_v values were significantly lower for MIF than for SIF motoneurons (1.02 ± 0.064 vs. 0.69 ± 0.059 spikes per second per degree per second, *n* = 81 and *n* = 40, for SIF and MIF motoneurons, respectively) (Fig. 6*F*) [*t*(119) = 3.239, *P* = 0.002, *t* test].

We also compared the goodness-of-fit of the multiple regression analysis performed between firing rate and eye position and velocity during vestibular eye movements. For this purpose, we compared

the coefficients of determination (R^2) of these regressions between SIF (0.779 ± 0.023) and MIF motoneurons (0.736 ± 0.038) motoneurons. There was no significant difference between R^2 of SIF versus MIF motoneurons [*t*(119) = 1.019, *P* = 0.31], therefore demonstrating that both motoneuronal types presented a robust eye position and eye velocity signal during vestibular eye movements.

Anatomical Distribution of Retrogradely Identified MIF Motoneurons in the Abducens Nucleus. For the morphological identification of MIF motoneurons, three animals were injected bilaterally into the myotendinous junction of the lateral rectus muscle with the retrograde tracer rhodamine (Rho). In all cases (six muscles) except one, the injection was limited to the myotendinous insertion without invading the belly where the end plates of the SIF motoneurons are located (at the middle third of the muscle) (13). Therefore, all of our morphological study was carried out in five abducens nuclei of three animals. Three examples of these injections are shown in Fig. 7*A*, *Top*, corresponding to the left lateral rectus muscle of each of the three animals.

The distribution of MIF motoneurons is shown for the left abducens nucleus of the three animals in Fig. 7*A* from caudal (top) to rostral (bottom). In all cases, choline acetyltransferase (ChAT) immunohistochemistry was also performed to identify the whole
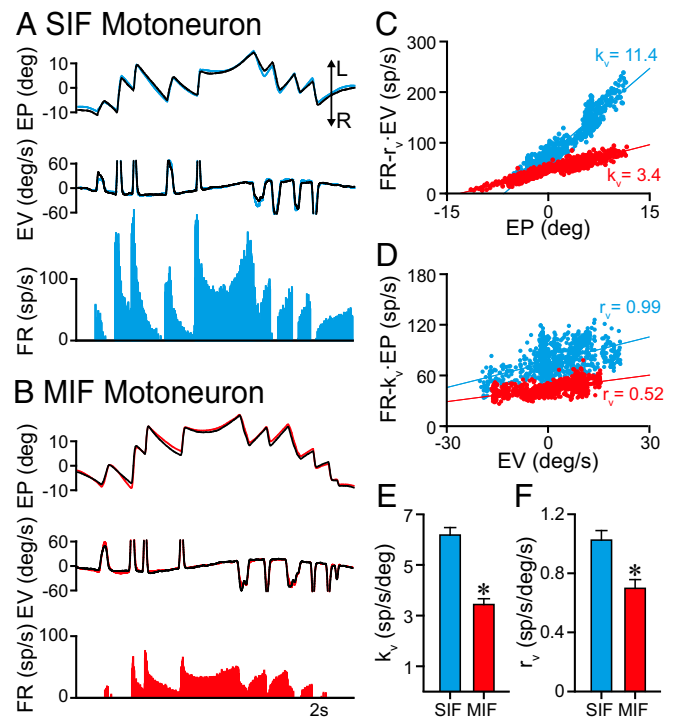
Fig. 6. Behavior of SIF and MIF motoneurons during vestibularly induced eye movements. (*A*) Firing rate of a SIF motoneuron recorded during vestibularly induced eye movements. The blue and the black traces correspond to the left and right eyes, respectively. (*B*) Same as *A*, but for a MIF motoneuron (left eye position in red). (*C*) Partial plot of the regression between firing rate (minus the velocity component, FR − $r_v \cdot EV$) and eye position for the SIF (blue dots and line) and the MIF (red dots and line) motoneurons illustrated in *A* and *B*, respectively. The eye position sensitivity during vestibularly induced eye movements (k_v) is indicated for each motoneuron. (*D*) Partial plot of the regression line between firing rate (minus the position component, FR − $k_v \cdot EP$) and eye velocity for the SIF (blue dots and line) and MIF (red dots and line) motoneurons illustrated in *A* and *B*, respectively. The eye velocity sensitivity during vestibularly induced eye movements (r_v) is indicated for each motoneuron. (*E* and *F*) Bar charts comparing k_v (*E*) and r_v (*F*) between SIF (*n* = 81) and MIF (*n* = 40) motoneurons. Data represent mean and SEM. Significant differences are indicated (**P* < 0.01, *t* test).
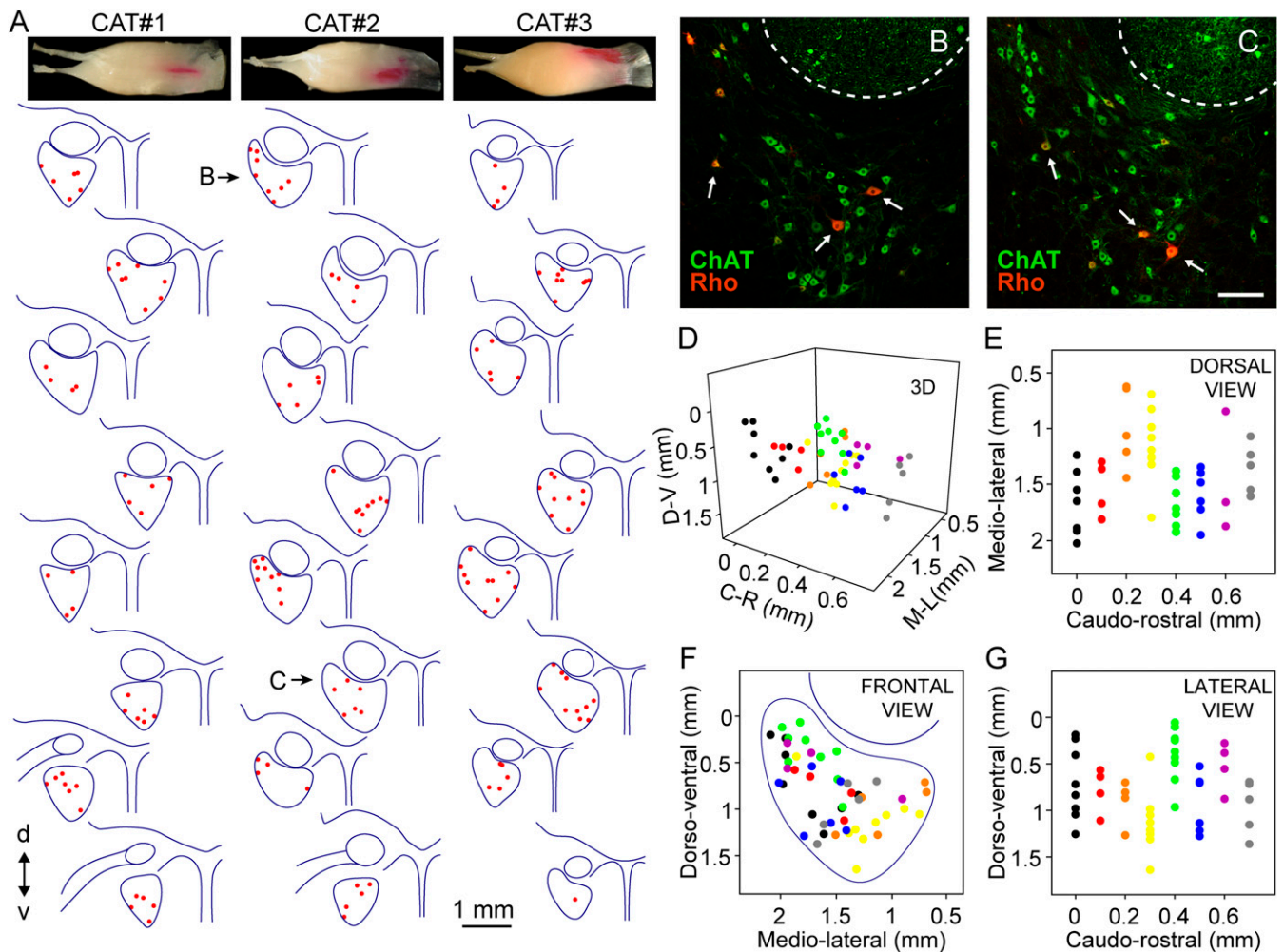
Fig. 7. Topographic distribution of MIF motoneurons. (*A*) Drawings of alternate coronal sections of the abducens nucleus from caudal (*Top*) to rostral (*Bottom*) of the three animals injected with Rho into the lateral rectus myotendinous junction to label MIF motoneurons (red dots). d, dorsal; v, ventral. (*B* and *C*) Images of the abducens nucleus after ChAT immunostaining (green) and retrograde Rho injection (Rho, red). Doubly labeled cells (ChAT$^+$ and Rho$^+$) correspond to MIF motoneurons (arrows). The dashed lines delineate the facial genu. These two images correspond to the drawings indicated in *A* as *B* and *C* for cat # 2. At the top of each of the three series the muscle injection for each cat is shown. (*D*) Graph showing the location of MIF motoneurons (colored dots) through the abducens nucleus in the three orthogonal axis (C-R, caudo-rostral; D-V, dorso-ventral; and M-L, medio-lateral) taking the most rostral point of the brainstem midline as the zero of coordinates. Eight colors were used to represent the location of MIF motoneurons; each color corresponds to each of the eight drawings shown for cat # 2 in *A*. (*E*–*G*) Planar representations of the graph shown in *D*. In *F* (same orientation as drawings in *A*), the limits of the abducens nucleus are indicated. (Scale bar, 200 μm for *B* and *C*.)

population of abducens motoneurons, and to delimit the boundaries of the nucleus. MIF motoneurons appeared doubly labeled (Rho$^+$, ChAT$^+$), whereas SIF motoneurons appeared unlabeled with respect to Rho but ChAT-immunostained. As appreciated in the images of the abducens nucleus (Fig. 7 *B* and *C*), Rho-retrogradely labeled cells (i.e., MIF motoneurons) were found intermingled with the Rho$^-$ but ChAT$^+$ cells (i.e., SIF motoneurons). Moreover, the topographic distribution of Rho$^+$ cells in the caudo-rostral series revealed no obvious distribution pattern. Thus, labeled motoneurons appeared located rostrocaudally, dorsoventrally, and mediolaterally throughout the abducens nucleus (Fig. 7*A*). To illustrate graphically the distribution of MIF motoneurons we elaborated a 3D plot indicating the location of MIF motoneurons in the three anatomical axis mentioned above (Fig. 7*D*), as well as the different planes of distribution according to every pair of axis (Fig. 7 *E*–*G*). Specifically, in Fig. 7*F* the location of MIF is illustrated dorsoventrally versus mediolaterally (i.e., as the drawings of Fig. 7*A*) and the limits of the abducens nucleus have also been outlined, illustrating that MIF motoneurons were scattered throughout the entire abducens nucleus.

We also calculated the percentage of MIF motoneurons with respect to the total population of abducens motoneurons as the percent of Rho-labeled cells in relation to the total number of abducens cells that appeared immunostained against ChAT. On average, we obtained that MIF motoneurons constituted 19.02% of the total motoneuronal population, in agreement with previous reports in monkeys (14) and rats (15).

Cell Size and Somatic Synaptic Coverage of SIF and MIF Motoneurons.
We compared the cell size of MIF and SIF motoneurons using the ChAT immunolabeling in both cell types. In particular, we measured the average cell diameter and somatic area. Visual inspection of MIF and SIF motoneurons in the histological sections showed cells of different sizes in the two motoneuronal populations, although the smallest cells tended to be MIF motoneurons. The distribution of average diameters showed that MIF motoneurons were shifted toward the left (smaller diameters) compared with SIF motoneurons, although there was considerable overlap of ranges (Fig. 8*A*). The average cell body
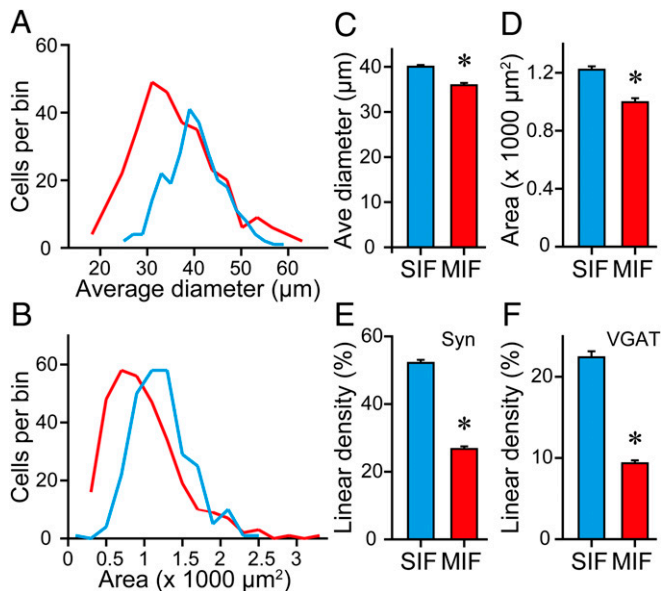
Fig. 8. Morphological features of SIF and MIF motoneurons. (*A* and *B*) Frequency distribution of average diameters (*A*) and somatic areas (*B*) of SIF (blue lines) and MIF (red lines) motoneurons. (*C*) Histogram of the average (Ave) diameter of SIF and MIF motoneurons. (*D*) Same as *C* but for cell body area (for *C* and *D*, n = 264 and 311 SIF and MIF motoneurons, respectively; *P < 0.001, t test). (*E*) Bar chart showing the synaptic coverage, calculated as the percent of cell body perimeter surrounded by synaptophysin (Syn)-immunoreactive boutons, in SIF and MIF motoneurons (n = 144 and 153 SIF and MIF motoneurons, respectively; *P < 0.001, t test). (*F*) Same as *E* but for VGAT synaptic coverage (n = 120 and 158 SIF and MIF motoneurons, respectively; *P < 0.001, t test).

diameter of MIF motoneurons was 35.98 ± 0.51 μm (n = 311 motoneurons) and that of SIF motoneurons was 40.09 ± 0.38 μm (n = 264), with MIF motoneurons being significantly smaller than SIF motoneurons (Fig. 8*C*) [$t(573) = -6.253$, P < 0.001, t test]. With the somatic area we obtained similar results (Fig. 8*B*). MIF motoneurons had a mean area of 998.76 ± 27.57 μm^2 (n = 311 motoneurons), which was significantly lower than that of SIF motoneurons ($1,222.85 \pm 23.06$ μm^2, n = 264) (Fig. 8*D*) [$t(573) = -6.106$, P < 0.001, t test].

We also quantified the percentage of the somatic perimeter covered by either synaptophysin- or vesicular GABA and glycine amino acid transporter (VGAT)-immunoreactive boutons, an index of the linear density of somatic boutons. We found that MIF motoneurons contained a significantly lower percentage of somatic synaptic boutons (labeled by synaptophysin) compared with SIF motoneurons (Figs. 8*E* and 9 *A–C*) [$26.73 \pm 0.76\%$, n = 153 cells, and $52.16 \pm 0.89\%$, n = 144, for MIF and SIF motoneurons, respectively; $t(295) = -21.782$, P < 0.001, t test]. Regarding inhibitory boutons, we obtained similar results (Fig. 9 *D–F*). Thus, MIF motoneurons contained an inhibitory synaptic coverage of $9.35 \pm 0.37\%$ (n = 158 cells), whereas the somatic perimeter of SIF motoneurons was covered by $22.40 \pm 0.74\%$ (n = 120), of VGAT-immunoreactive boutons (Fig. 8*F*) [$t(276) = -16.993$, P < 0.001, t test].

The percentage of inhibitory boutons (VGAT-immunoreactive) with respect to the total percentage of synaptophysin-labeled boutons terminating on MIF or SIF motoneurons showed a similar inhibitory-to-total synaptic coverage in MIF in relation to SIF motoneurons [$0.35 \pm 0.01\%$ versus $0.40 \pm 0.02\%$, respectively, n = 5 abducens nuclei; $t(8) = -2.108$, P = 0.068, t test]. These results indicated that the inhibitory-to-excitatory balance in somatic synaptic boutons was similar for both motoneuronal types.

Discussion

The present work has demonstrated that MIF and SIF motoneurons of the cat abducens nucleus display an eye position and an eye velocity sensitivity during different types of eye movements, indicating that they share a similar firing pattern composed of both a static and a dynamic component. However, we found significant differences in eye-related parameters between both motoneuronal types. Thus, MIF motoneurons presented lower eye position and velocity sensitivities, discharging at lower rates than SIF motoneurons, as well as lower recruitment thresholds. Accordingly, our data cannot support a physiological segregation between MIF and SIF motoneurons based on the type of eye movement. The retrograde labeling of MIF abducens motoneurons revealed that they were not segregated anatomically either. MIF motoneurons, however, were smaller and showed a lesser density of synapses contacting their cell bodies (Fig. 10).

Similarities and Differences in Discharge Activity Between MIF and SIF Motoneurons. Previous studies in monkeys using retrograde transneuronal transfer of rabies virus have demonstrated quantitative
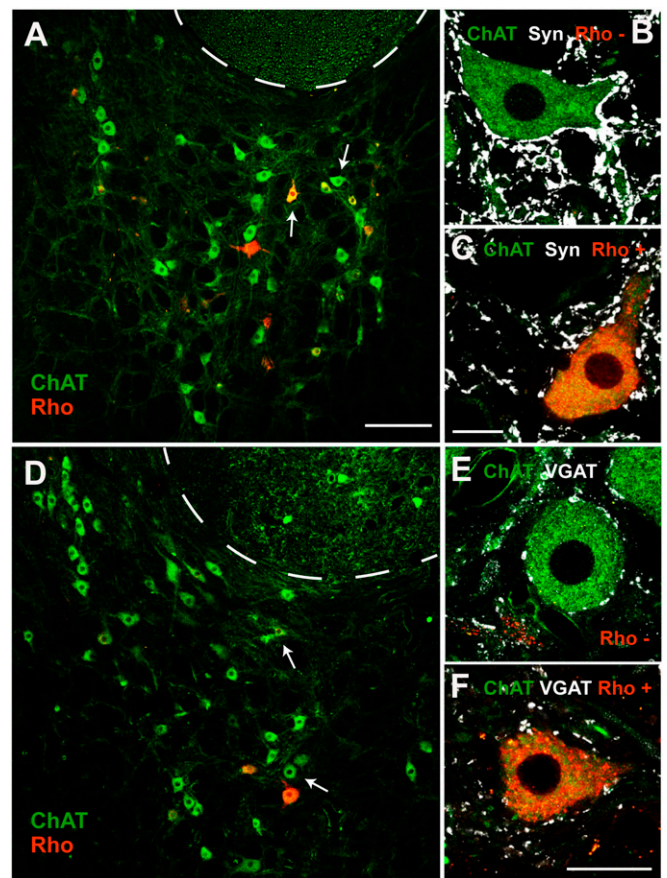

Fig. 9. Synaptic coverage of SIF and MIF motoneurons. (*A*) Image of the abducens nucleus after immunostaining against ChAT (green). MIF motoneurons are the Rho$^+$ cells (red). The cells indicated by white arrows in *A* are illustrated at higher magnification in *B* and *C*, respectively. (*B*) Example of a Rho$^-$ SIF motoneuron after double immunolabeling against ChAT (green) and synaptophysin (white). (*C*) Same as *B* but for a Rho$^+$ MIF motoneuron. Note the higher density of synaptic boutons contacting the soma of the SIF motoneuron in *B* compared with the MIF motoneuron in *C*. (*D–F*) Same as *A–C*, but after VGAT immunolabeling (white) as a marker of inhibitory synaptic boutons. In addition, the SIF motoneuron was contacted perisomatically by more VGAT$^+$ boutons (in *E*) than the MIF motoneuron (in *F*). [Scale bars: 200 μm in *A* (for *A* and *D*); 20 μm in *C* (for *B*, *C*, and *E*); 20 μm in *F*.]
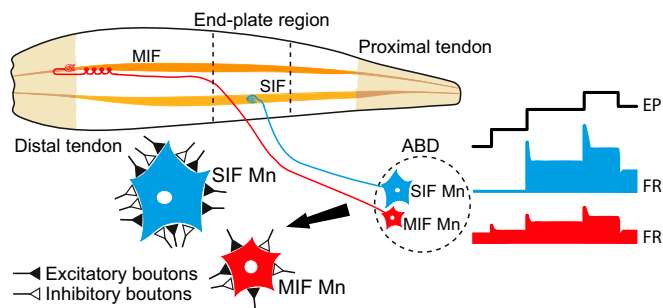
Fig. 10. Summary of results. The abducens nucleus (ABD) contains SIF (in blue) and MIF (in red) motoneurons (Mn). SIF motoneurons terminate on SIF fibers forming the typical *en plaque* neuromuscular junction in the end-plate region of the lateral rectus muscle. MIF motoneurons establish multiple synaptic boutons *en grappe* extending along the fiber (only the distal part is illustrated). These axons also form the so-called palisade endings at the myotendinous junction. We have demonstrated that MIF motoneurons have an overall lower firing rate, smaller eye position, and eye velocity sensitivities, bursts of lower frequency during on-directed saccades, and lower recruitment thresholds than SIF motoneurons. MIF and SIF motoneurons participated in all types of eye movement studied herein. MIF motoneurons also had a smaller soma size and less somatic boutons. On the other hand, both MIF and SIF motoneurons showed a similar ratio of excitatory-to-inhibitory synaptic boutons.

differences in monosynaptic inputs to MIF and SIF motoneurons of the abducens nucleus (21). The premotor connectivity of MIF motoneurons arises predominantly from structures carrying eye position or slow eye velocity, such as during vergence, which has led to propose that MIF motoneurons would be involved in fixations without participating in fast eye movements, like saccades and the vestibulo-ocular reflex. Similar conclusions have been proposed after anterograde labeling from several premotor areas to SIF and MIF oculomotor motoneurons in monkeys (20). More recent studies have also found differences in afferents to the two motoneuronal types (22, 23). Our data, however, are not in accordance with the division of motoneurons into "slow" versus "fast" or "tonic" versus "phasic," nor in a segregation based on the type of eye movement in which they participate (15, 20, 21, 31). Indeed, we found that the two types of motoneuron participated in different types of eye movements such as saccades, the vestibulo-ocular reflex, vergence, and fixations.

It should be noted, however, that we found significant physiological differences that could be in accordance with previous morphological studies (20–23). The analysis of discharge characteristics revealed noticeably lower firing rates in MIF motoneurons compared with SIF motoneurons. Of special relevance was the presence in MIF motoneurons of bursts of spikes of low frequency during on-directed saccades, which markedly contrasted with those of SIF motoneurons. The same happened for eye fixations. Taken together, our physiological findings did not distinguish between tonic versus phasic motoneurons, but they clearly separated these two motoneuronal populations based on their eye position and eye velocity sensitivities. Moreover, the differences found in sensitivities (position and velocity), F_o, and recruitment threshold between MIF and SIF abducens motoneurons could indicate that MIF motoneurons might be controlling mainly movements where the changes in muscle tension per degree of eye movement are subtle (i.e., when gaze is nasally oriented). In contrast, as the gaze moves toward temporal positions, larger increments of tension per degree are needed (27), and therefore SIFs abducens motoneurons would be recruited.

In agreement with previous single-unit studies carried in rabbits, cats, and monkeys, we found that each motoneuron recorded participates in every type of eye movement, exhibiting a tonic–phasic discharge pattern (24–28, 32–34). Electromyo-

graphic recordings from human extraocular muscles have also shown that all muscle fibers contribute to different types of eye movements (35).

MIF Motoneuron Cell Bodies Are Smaller and Receive Fewer Synaptic Boutons. In agreement with previous studies, we have found that the cell bodies of MIF motoneurons were smaller than those of SIF motoneurons (14, 16, 19, 20, 36). It has also been reported that MIF axons and fibers are smaller (2, 4, 9). The smaller size of MIF cells could explain the significantly longer antidromic activation latencies found in MIF versus SIF motoneurons, as well as their lower recruitment threshold, because smaller neurons, with higher input resistance, tend to be more excitable for a given amount of synaptic current.

Our analysis of the somatic synaptic coverage revealed a larger density of synapses on SIF compared with MIF motoneurons in agreement with previous studies in monkeys showing that the groups A and B (SIF) of medial rectus motoneurons receive numerous somatic contacts, in marked contrast with the C group (MIF) (36). Altogether, these data likely indicate a major synaptic drive of SIF motoneurons, which could correlate with their higher firing rates and sensitivities that we describe here. Moreover, both MIF and SIF motoneurons have been shown to receive the same types of afferent, although in different proportions (20, 21).

Both types of motoneuron received somatic inhibitory boutons (VGAT-immunoreactive). At least part of these inhibitory boutons could arise from inhibitory burst neurons described to contact mainly the soma of abducens neurons (37–40). These findings could explain the rapid inhibition observed in the discharge of not only SIF, as expected, but also MIF motoneurons during off-directed saccades. Therefore, MIF motoneurons clearly encoded the appropriate signals during on- and off-directed saccades.

Our morphological study also demonstrated that MIF and SIF motoneurons appeared intermingled within the cat abducens nucleus, in contrast with previous studies in monkeys and rats, where it has been described a peripheral location for MIF motoneurons (15–17, 36). However, the specific retrograde labeling of motoneurons from the orbital versus the global layer of the lateral rectus muscle in cats has also revealed that both pools are randomly distributed within the abducens nucleus (19).

Functional Implications. There is a consensus regarding the participation of SIF motoneurons in the different types of eye movements and our data corroborate this assumption. The finding that SIF motoneurons had higher recruitment thresholds and sensitivities suggests that they could contribute mainly to increase muscle tension as gaze is deviated more in the on-direction, when more force is needed. On the other hand, MIF motoneurons innervate muscle fibers characterized by the absence of a twitch in response to a single stimulus. During repetitive stimulation, however, these fibers generate a tension that increases with stimulus rate (41). We have found that nontwitch fibers are innervated by low threshold (MIF) motoneurons, as previously suggested (24, 32), having low position and velocity sensitivities and lower recruitment thresholds. Altogether, it might be surmised that MIF motoneurons contribute with a continuous and finely graded firing that would be necessary for the exquisite precision of eye position in the orbit during the different types of eye movement.

It has long been envisaged a matching of filter-firing properties from the primary vestibular afferents into the MIF and SIF motoneurons (42). This proposal, later termed "frequency-selective channels," arose from the observation that there were frequency-selective changes during adaptation of the vestibulo-ocular gain (43). Thus, the parallel processing of vestibular signals is a common organizational property of vertebrates where

hair cells, primary afferents, and second-order vestibular neurons are classified as having different response dynamics, frequency selectivity, synaptic receptors, and intrinsic properties (44). The most explicit demonstration of parallel channels from vestibular cells to motoneurons arises from the frog (45). The linkage of silent and tonically active motoneurons within two groups matches with the general concept of twitch versus tonic motoneurons (15, 31). Our data indicate that the semantic separation of tonic and phasic groups can be better extrapolated into a continuum spectrum of sensitivities and thresholds through the motoneuronal pool. However, we have described that the two groups of motoneurons have statistically different discharge characteristics.

Another important aspect concerning MIF motoneurons is that they seem to be the origin of palisade endings, as we demonstrated in Zimmermann et al. (46), although the technique used did not allow us to determine whether all palisade endings arise from MIF axons (47). Support that palisade endings are an expansion of MIF motoneurons came also from a developmental study, where we showed that axons with multiple motor contacts grow out into the tendon and turn back to form palisade endings at the muscle fiber tips (48). Palisade endings are unique nerve specializations in extraocular muscles and consist of a cuff of nerve terminals around the tip of some MIFs (49, 50).

Different to a MIF/palisade ending construction, other authors (51, 52) have suggested that palisade endings and MIFs originate from different pools of neurons at the periphery of the extraocular motor nuclei. Specifically, palisade endings originate from spindle-shaped sensor-like neurons and MIFs from multipolar motor-like neurons. If such different neuronal populations are present in the cat abducens nucleus, we should have antidromically activated both from our stimulating electrode placed at the myotendinous junction. It should be pointed out that we did not find two different firing patterns in our cells activated from the electrode at the lateral rectus insertion. Therefore, our data suggest the existence of a unique population of abducens neurons, likely giving rise to both *en grappe* terminals and palisade endings. Palisade endings are enigmatic structures because they exhibit sensory as well as motor features: that is, they have nerve terminals contacting the tendon, which is in analogy to sensory Golgi tendon organs, but they are cholinergic and originate from the extraocular motor nuclei, which is more compatible with motor features. To date, the function of palisade endings is still elusive, and clearly more research is needed to unravel the function of palisade endings and their relation to MIF motoneurons.

Materials and Methods

Ethics Statement. All procedures were performed in accordance with the guidelines of the European Union (2010/63/EU) and the Spanish legislation (R.D. 53/2013, BOE 34/11370–421) for the use and care of laboratory animals, and approved by the ethics committee of the Universidad de Sevilla and Junta de Andalucía (Protocol #13/04/2018/047). All efforts were made to reduce the number of animals used.

Animals and Surgical Procedures. Experiments were performed on adult female cats weighing 2.0–2.5 kg obtained from authorized suppliers (Universidad de Córdoba, Spain). A total of five cats was used for the present study. Four of them were used for recordings. For morphology, we used two of the recorded animals and one additional cat not used for recordings. Animals received a protective injection of atropine sulfate (0.5 mg/kg, intramuscularly), and then were anesthetized with ketamine hydrochloride (20 mg/kg, intramuscularly) mixed with xylazine (0.5 mg/kg, intramuscularly). Stereotaxic surgery was performed to implant intracranially two bipolar electrodes in both VIth nerves. Electrodes were made of 200-μm polyimide insulated silver wire (California Fine Wire). In addition, a pair of hook-electrodes made of three-strand stainless steel Teflon insulated was inserted at the myotendinous junction of the left lateral rectus muscle (A-M systems). Coils, made up of two turns of Teflon-isolated multistranded stainless-steel wire, were implanted in the sclera of both eyes (Cooner Wire). For recordings, a square window (5 mm²) was drilled in the occipital bone, which was aseptically sealed between recording sessions.

Chronic Extracellular Recordings. After 10 days of postoperative recovery, recording sessions started. The animal was gently restrained with elastic bandages and head-fixed inside the magnetic field for eye movement recordings (53). Extracellular recordings were carried out with glass micropipettes, filled with 2 M sodium chloride. The (left) abducens nucleus was identified by the antidromic field potential recorded following the electrical stimulation (50-μs pulses of <0.1 mA) to the ipsilateral VIth nerve. MIF and SIF abducens motoneurons were antidromically identified from the VIth nerve. Those cells that were also activated from the myotendinous junction were considered MIF motoneurons. Collision test of the orthodromic and antidromic spike was also applied sistematically. Once identified, the extracellular action potentials of the motoneuron were recorded during spontaneous eye movements. For most cells, it was also possible to study their behavior during vestibularly induced eye movements.

Data Storage and Analysis. Neuronal activity along with the horizontal eye position of both eyes were digitally stored for off-line analysis (Power 1401; Cambridge Electronic Design). The firing rate of abducens motoneurons can be correlated to both eye position and eye velocity according to the equation $FR = F_0 + k \cdot EP + r \cdot EV$, where k and r are the position and velocity neuronal sensitivities, respectively, and F_0 is the firing rate at straight-ahead gaze (i.e., when $EP = 0°$) (24, 26, 27). During eye fixations, because $EV = 0$, the former equation can be expressed as $FR = F_0 + k \cdot EP$, and thus motoneuronal FR can be fitted to eye position by a linear regression line, whose slope represents the neuronal eye position sensitivity during spontaneous fixations, hereafter named k_s (in spikes per second per degree). We avoided the postsaccadic slide effect on firing rate by sampling stationary data during the fixation. To calculate the motoneuronal eye velocity sensitivity during spontaneous rapid eye movements or saccades, we subtracted to FR the position component ($k_s \cdot EP$) calculated from the previously known sensitivity to EP. Thus, the equation used was $FR - k_s \cdot EP = F_0 + r_v \cdot EV$. The slope of the linear regression line obtained by this method corresponds to the neuronal eye velocity sensitivity during saccades, r_s (in spikes per second per degree per second). During vestibularly induced eye movements, we used multiple regression analysis to correlate FR with EP and EV, selecting only the slow phases of the nystagmus. Therefore, the equation used was $FR = F_0 + k_v \cdot EP + r_v \cdot EV$, where k_v (in spikes per second per degree) and r_v (in spikes per second per degree per second) correspond to the neuronal eye position and velocity sensitivities, respectively, during vestibularly induced eye movements. We avoided the initial 150 ms after the fast phases to reduce the influence of the postsaccadic slide in the data.

Retrograde Labeling of Motoneurons. Under general anesthesia (same as above), the lateral rectus muscle was dissected and held by the tendon with a muscle hook. Using a Hamilton syringe, 1 μL of 20% rhodamine B isothiocyanate (Sigma-Aldrich) dissolved in 2% dimethyl sulfoxide was injected at the myotendinous junction of the lateral rectus muscle bilaterally to selectively label only MIF motoneurons, as previously described (15, 16, 19). After a survival period of 6–9 days, animals received terminal anesthesia with sodium pentobarbital (100 mg/kg, i.p.) and were transcardially perfused with 500 mL of saline followed by 2 L of fixative consisting in 4% paraformaldehyde prepared in 0.1 M phosphate buffer, pH 7.4. The brainstem was cut coronally with a vibratome into 50-μm-thick sections.

Immunofluorescence. For each animal, two parallel series of histological sections from the most caudal up to the most rostral end of the abducens nucleus were processed for double immunofluorescence. In one series, we combined ChAT (to label the motoneurons) with synaptophysin (as a marker of synaptic boutons) immunolabeling. In the other series, we combined ChAT with VGAT (inhibitory bouton marker). Primary antibodies used were: (*i*) goat polyclonal antibody against ChAT (1:500; Millipore); (*ii*) mouse monoclonal antibody against synaptophysin (1:1,000; Millipore); and (*iii*) rabbit polyclonal antibody against VGAT (1:500; Millipore). Secondary antibodies (Jackson ImmunoResearch) used at a dilution 1:50 were the following: (*i*) donkey anti-goat IgG coupled to FITC (for ChAT detection); (*ii*) donkey anti-mouse IgG coupled to Cy5 (to reveal synaptophysin); and (*iii*) donkey anti-rabbit IgG coupled to Cy5 (for VGAT detection). A confocal microscope and ZEN software were used (Zeiss LSM 7 DUO). Gray scales were adjusted to expand the maximum dynamic range of the image.

Morphological Analysis. Confocal microscope images were used to measure: (*i*) the topographic distribution of identified motoneurons; (*ii*) their cell size; and (*iii*) their synaptic coverage with synaptophysin or VGAT. Doubly labeled motoneurons (ChAT and Rho), were considered MIF motoneurons. Rho⁻ but Chat⁺ motoneurons were considered SIF motoneurons. The distribution of

MIF motoneurons was drawn in Adobe illustrator (Adobe Systems) using 4 × 4 tile confocal images at 10× magnification in all sections containing the abducens nucleus. To estimate the proportion of MIF and SIF motoneurons we performed cells counts considering only those neurons showing a clearly visible nucleus. To measure the somatic size of motoneurons, stacks of focal planes of 1-μm virtual thickness were captured at 63× magnification. We chose the plane in which the motoneuron exhibited its nucleus at its maximum diameter. Using ImageJ (NIH), we measured the average diameter, the perimeter, and the area of the cell bodies of motoneurons. Synaptic coverage was calculated as the percentage of the somatic perimeter that appeared surrounded by either synaptophysin or VGAT synaptic boutons.

Statistics. Comparisons between groups were performed using the Student t test at a level of significance of $P < 0.05$ by means of the statistics program SigmaPlot 11 (Systat Software, Inc.). When required, we also used the two-way ANOVA test using the Holm–Sidak method for post hoc all pairwise multiple comparisons. Data were represented as mean $\pm$ SEM. All regression analysis used in the present study were significant ($P < 0.05$).

1. Hess A, Pilar G (1963) Slow fibres in the extraocular muscles of the cat. *J Physiol* 169: 780–798.
2. Namba T, Nakamura T, Takahashi A, Grob D (1968) Motor nerve endings in extraocular muscles. *J Comp Neurol* 134:385–396.
3. Mayr R (1971) Structure and distribution of fibre types in the external eye muscles of the rat. *Tissue Cell* 3:433–462.
4. Nelson JS, Goldberg SJ, McClung JR (1986) Motoneuron electrophysiological and muscle contractile properties of superior oblique motor units in cat. *J Neurophysiol* 55:715–726.
5. Shall MS, Goldberg SJ (1992) Extraocular motor units: Type classification and motoneuron stimulation frequency-muscle unit force relationships. *Brain Res* 587:291–300.
6. Bondi AY, Chiarandini DJ (1983) Morphologic and electrophysiologic identification of multiply innervated fibers in rat extraocular muscles. *Invest Ophthalmol Vis Sci* 24:516–519.
7. Bach-y-Rita P, Ito F (1966) In vivo studies on fast and slow muscle fibers in cat extraocular muscles. *J Gen Physiol* 49:1177–1198.
8. Pilar G (1967) Further study of the electrical and machanical responses of slow fibers in cat extraocular muscles. *J Gen Physiol* 50:2289–2300.
9. Browne JS (1976) The contractile properties of slow muscle fibres in sheep extraocular muscle. *J Physiol* 254:535–550.
10. Schiaffino S, Reggiani C (2011) Fiber types in mammalian skeletal muscles. *Physiol Rev* 91:1447–1531.
11. Morgan DL, Proske U (1984) Vertebrate slow muscle: Its structure, pattern of innervation, and mechanical properties. *Physiol Rev* 64:103–169.
12. Porter JD, Baker RS, Ragusa RJ, Brueckner JK (1995) Extraocular muscles: Basic and clinical aspects of structure and function. *Surv Ophthalmol* 39:451–484.
13. Spencer RF, Porter JD (2006) Biological organization of the extraocular muscles. *Prog Brain Res* 151:43–80.
14. Eberhorn AC, Ardeleanu P, Büttner-Ennever JA, Horn AK (2005) Histochemical differences between motoneurons supplying multiply and singly innervated extraocular muscle fibers. *J Comp Neurol* 491:352–366.
15. Eberhorn AC, Büttner-Ennever JA, Horn AK (2006) Identification of motoneurons supplying multiply- or singly-innervated extraocular muscle fibers in the rat. *Neuroscience* 137:891–903.
16. Büttner-Ennever JA, Horn AK, Scherberger H, D'Ascanio P (2001) Motoneurons of twitch and nontwitch extraocular muscle fibers in the abducens, trochlear, and oculomotor nuclei of monkeys. *J Comp Neurol* 438:318–335.
17. Tang X, Büttner-Ennever JA, Mustari MJ, Horn AK (2015) Internal organization of medial rectus and inferior rectus muscle neurons in the C group of the oculomotor nucleus in monkey. *J Comp Neurol* 523:1809–1823.
18. Horn AKE, Horng A, Buresch N, Messoudi A, Härtig W (2018) Identification of functional cell groups in the abducens nucleus of monkey and human by perineuronal nets and choline acetyltransferase immunolabeling. *Front Neuroanat* 12:45.
19. Bohlen MO, Warren S, Mustari MJ, May PJ (2017) Examination of feline extraocular motoneuron pools as a function of muscle fiber innervation type and muscle layer. *J Comp Neurol* 525:919–935.
20. Wasicky R, Horn AK, Büttner-Ennever JA (2004) Twitch and nontwitch motoneuron subgroups in the oculomotor nucleus of monkeys receive different afferent projections. *J Comp Neurol* 479:117–129.
21. Ugolini G, et al. (2006) Horizontal eye movement networks in primates as revealed by retrograde transneuronal transfer of rabies virus: Differences in monosynaptic input to "slow" and "fast" abducens motoneurons. *J Comp Neurol* 498:762–785.
22. Bohlen MO, Warren S, May PJ (2017) A central mesencephalic reticular formation projection to medial rectus motoneurons supplying singly and multiply innervated extraocular muscle fibers. *J Comp Neurol* 525:2000–2018.
23. Prevosto V, Graf W, Ugolini G (2017) The control of eye movements by the cerebellar nuclei: Polysynaptic projections from the fastigial, interpositus posterior and dentate nuclei to lateral rectus motoneurons in primates. *Eur J Neurosci* 45:1538–1552.
24. Robinson DA (1970) Oculomotor unit behavior in the monkey. *J Neurophysiol* 33:393–403.
25. Schiller PH (1970) The discharge characteristics of single units in the oculomotor and abducens nuclei of the unanesthetized monkey. *Exp Brain Res* 10:347–362.
26. Delgado-García JM, del Pozo F, Baker R (1986) Behavior of neurons in the abducens nucleus of the alert cat—I. Motoneurons. *Neuroscience* 17:929–952.
27. Davis-López de Carrizosa MA, Morado-Díaz CJ, Miller JM, de la Cruz RR, Pastor AM (2011) Dual encoding of muscle tension and eye position by abducens motoneurons. *J Neurosci* 31:2271–2279.
28. Pastor AM, González-Forero D (2003) Recruitment order of cat abducens motoneurons and internuclear neurons. *J Neurophysiol* 90:2240–2252.
29. Henneman E, Somjen G, Carpenter DO (1965) Functional significance of cell size in spinal motoneurons. *J Neurophysiol* 28:560–580.
30. Zhou W, King WM (1998) Premotor commands encode monocular eye movements. *Nature* 393:692–695.
31. Büttner-Ennever JA, Horn AK (2002) The neuroanatomical basis of oculomotor disorders: The dual motor control of extraocular muscles and its possible role in proprioception. *Curr Opin Neurol* 15:35–43.
32. Fuchs AF, Scudder CA, Kaneko CR (1988) Discharge patterns and recruitment order of identified motoneurons and internuclear neurons in the monkey abducens nucleus. *J Neurophysiol* 60:1874–1895.
33. Fuchs AF, Luschei ES (1970) Firing patterns of abducens neurons of alert monkeys in relationship to horizontal eye movement. *J Neurophysiol* 33:382–392.
34. Stahl JS, Simpson JI (1995) Dynamics of abducens nucleus neurons in the awake rabbit. *J Neurophysiol* 73:1383–1395.
35. Scott AB, Collins CC (1973) Division of labor in human extraocular muscle. *Arch Ophthalmol* 90:319–322.
36. Erichsen JT, Wright NF, May PJ (2014) Morphology and ultrastructure of medial rectus subgroup motoneurons in the macaque monkey. *J Comp Neurol* 522:626–641.
37. Hikosaka O, Igusa Y, Nakao S, Shimazu H (1978) Direct inhibitory synaptic linkage of pontomedullary reticular burst neurons with abducens motoneurons in the cat. *Exp Brain Res* 33:337–352.
38. Destombes J, Rouvière A (1981) Ultrastructural study of vestibular and reticular projections to the abducens nucleus. *Exp Brain Res* 43:253–260.
39. Langer T, Kaneko CR, Scudder CA, Fuchs AF (1986) Afferents to the abducens nucleus in the monkey and cat. *J Comp Neurol* 245:379–400.
40. Escudero M, Delgado-García JM (1988) Behavior of reticular, vestibular and prepositus neurons terminating in the abducens nucleus of the alert cat. *Exp Brain Res* 71:218–222.
41. Meredith MA, Goldberg SJ (1986) Contractile differences between muscle units in the medial rectus and lateral rectus muscles in the cat. *J Neurophysiol* 56:50–62.
42. Baker R, Evinger C, McCrea RA (1981) Some thoughts about the three neurons in the vestibular ocular reflex. *Ann N Y Acad Sci* 374:171–188.
43. Lisberger SG, Miles FA, Optican LM (1983) Frequency-selective adaptation: Evidence for channels in the vestibulo-ocular reflex? *J Neurosci* 3:1234–1244.
44. Straka H, Vibert N, Vidal PP, Moore LE, Dutia MB (2005) Intrinsic membrane properties of vertebrate vestibular neurons: Function, development and plasticity. *Prog Neurobiol* 76:349–392.
45. Dietrich H, Glasauer S, Straka H (2017) Functional organization of vestibulo-ocular responses in abducens motoneurons. *J Neurosci* 37:4032–4045.
46. Zimmermann L, et al. (2013) Axons giving rise to the palisade endings of feline extraocular muscles display motor features. *J Neurosci* 33:2784–2793.
47. Rao HM, Prevosto V (2013) Proprioceptive eye position signals are still missing a sensory receptor. *J Neurosci* 33:10585–10587.
48. Blumer R, Streicher J, Davis-López de Carrizosa MA, de la Cruz RR, Pastor AM (2017) Palisade endings of extraocular muscles develop postnatally following different time courses. *Invest Ophthalmol Vis Sci* 58:5105–5121.
49. Ruskell GL (1978) The fine structure of innervated myotendinous cylinders in extraocular muscles of rhesus monkeys. *J Neurocytol* 7:693–708.
50. Alvarado-Mallart RM, Pinçon-Raymond M (1979) The palisade endings of cat extraocular muscles: A light and electron microscope study. *Tissue Cell* 11:567–584.
51. Lienbacher K, Mustari M, Hess B, Büttner-Ennever J, Horn AK (2011) Is there any sense in the palisade endings of eye muscles? *Ann N Y Acad Sci* 1233:1–7.
52. Lienbacher K, Horn AK (2012) Palisade endings and proprioception in extraocular muscles: A comparison with skeletal muscles. *Biol Cybern* 106:643–655.
53. Fuchs AF, Robinson DA (1966) A method for measuring horizontal and vertical eye movement chronically in the monkey. *J Appl Physiol* 21:1068–1070.